Exploring the non-covalent interactions behind the formation of amine–water complexes: The case of the *N*-allylmethylamine monohydrate

Weslley G. D. P. Silva, Tamanna Poonia and Jennifer van Wijngaarden*

Department of Chemistry, University of Manitoba, Winnipeg, Manitoba, R3T 2N2, Canada

*Corresponding author

Email: vanwijng@cc.umanitoba.ca

Phone: (204)474-8379

Fax: (204)474-7608

Abstract

The conformational landscape of the monohydrated complex of *N*-allylmethylamine (AMA–w) was investigated for the first time using rotational spectroscopy from 8–20 GHz and quantum chemistry calculations. From a total of nine possible energy minima within 10 kJ mol^{-1}, transitions for the two most stable conformers of AMA–w were detected, and assigned aided by DFT and *ab* initio MP2 predictions. The observed rotational transitions displayed characteristic hyperfine splittings due to the presence of the ^{14}N quadrupolar nucleus. Quantum theory of atoms in molecules (QTAIM), non-covalent interaction (NCI) and natural bond orbital (NBO) analyses showed that the observed conformers of AMA–w are stabilized by two intermolecular interactions consisting of a dominant N···H–O and a secondary C–H···O hydrogen bond (HB) in which the water molecule acts simultaneously as a HB donor and acceptor. The HBs formed with water do not change the relative energy ordering of the most stable conformers of AMA but do affect the stability of higher energy conformations by disrupting the intramolecular forces responsible for their geometries. By comparing the intermolecular interaction energies with those of the monohydrates of the simplest primary (methylamine, MA), secondary (dimethylamine, DMA) and tertiary (trimethylamine, TMA) amines using symmetry-adapted perturbation theory (SAPT) calculations, we find that AMA forms the strongest bound complex with water. This is rationalized through the identification of subtle differences in stabilizing and destabilizing contributions across the amine–w series of complexes.

Introduction

A comprehensive understanding of the non-covalent interactions governing the stability of hydrates is of great interest because of the ubiquitous nature of water. Molecular aggregates formed between water and amines, for example, play a crucial role in biology—being essential to the existence of life—and in the chemistry of the atmosphere where amines are involved in key processes such as aerosol nucleation.[1] The undeniable importance of these clusters has motivated both theoretical and spectroscopic studies[2–8] of the hydrogen bonding networks between the amino group and water which have largely focused on water microsolvation of small N-containing molecules such as ammonia (ammonia–w),[2,3] methylamine (MA–w),[5] dimethylamine (DMA–w)[4–6] and trimethylamine (TMA–w).[7,8] These reports have shown that the interaction between the water molecule and the amino group occurs via an intermolecular N···H–O hydrogen bond (HB) in which the water typically acts as the HB donor while the N serves as a HB acceptor. The strength of the binding interactions increases with the number of methyl substituents around the N atom following a general stability trend of TMA–w > DMA–w > MA–w > ammonia–w.

Chen *et al*[9] evaluated the impact of two larger alkyl substituents on the HB parameters of primary amine–w complexes by studying *n*-propylamine–water (PA–w) and isopropylamine–water (IPA–w) using computational chemistry and rotational spectroscopy. It was found that the larger side chains of PA and IPA in comparison to that of MA and ethylamine do not have a significant impact on the interaction energies of the monohydrates.[9] These findings provide useful information to understand binding involving larger alkyl primary amines such as those present in biological environments. Investigation of the monohydrates of secondary and tertiary amines is essential to the

development of a systematic understanding of the influence of diverse side chains on the formation of amine–w clusters. This enhanced knowledge promises to shed light on the fundamental processes driving the chemistry of amines in aqueous environments.

N-allylmethylamine (CH_2=CH–CH_2–NH–CH_3, AMA) is an amine of astrochemical and atmospheric relevance.[10,11] A recent microwave spectroscopic study[10] reported transitions belonging to four conformers in the rotational spectrum of AMA whose stabilities have been rationalized by a complex interplay between steric and attractive interactions. The examination of the AMA–w complex is a crucial first step to understanding the changes in its conformational behaviour in the presence of water and to elucidate the effect of the allyl group on the intermolecular interaction. In comparison to the simplest secondary amine DMA, the presence of the vinyl substituent in AMA may alter the electron density around N through intramolecular interaction and offers an additional potential binding site for the water molecule which would directly impact the interaction energy of the AMA–w complex.

In this study, we investigated the conformational behaviour of AMA–w for the first time using a combination of rotational spectroscopy and high-level quantum chemical calculations. Transitions arising from two unique conformers of the complex were observed in the rotational spectrum and their assignments were confirmed by the presence of a hyperfine splitting related to the quadrupolar ^{14}N nucleus. To understand the nature of the intra- and intermolecular interactions that govern the observed conformers, we used quantum theory of atoms in molecules (QTAIM),[12] non-covalent interaction (NCI)[13] and natural bond orbital (NBO)[14] analyses. The interaction energies were decomposed into four components (electrostatic, dispersion, induction and

exchange or Pauli repulsion) using symmetry-adapted perturbation theory (SAPT)[15] calculations and the results compared with those derived in this work for the water dimer, ammonia–w, MA–w, DMA–w and TMA–w.

Experimental methods

AMA (96%, bp: 334–335 K) is commercially available from Alfa Aesar and was used without further purification. To produce the monohydrated complex, a gas mixture containing ~1% of AMA in neon (100 kPa) was prepared at room temperature and subsequently bubbled through a reservoir containing water. The mixture (AMA + water) was then delivered to the high vacuum ($P \approx 10^{-7}$ kPa) chamber of the instruments via a supersonic jet expansion through a pulsed nozzle (1 mm diameter). Rotational spectra of the complex were collected using a chirped-pulse (cp) and a Balle-Flygare (BF) Fourier transform microwave (FTMW) spectrometer which have been described in detail previously.[16,17] Initial measurements were performed using the cp-FTMW instrument to record a broadband spectrum from 8–18 GHz in segments of 2 GHz each. On the basis of the survey spectra, the most intense rotational transitions belonging to the different conformers of the AMA–w complex were identified. These transitions showed partially resolved hyperfine splittings due to the presence of the ^{14}N quadrupolar nucleus. Final frequency measurements were performed using the BF-FTMW spectrometer (8–20 GHz) which features higher resolution and sensitivity. This allowed the hyperfine structure to be better resolved and the less intense spectral features to be recorded. Transitions collected with the BF-FTMW instrument have linewidths (FWHM) of ~7 kHz while the uncertainty in the line positions is ±2 kHz. In the BF-FTMW setup, all transitions are split

into two Doppler components due to the coaxial arrangement of the molecular beam and the resonator axis.

Computational methods

To identify possible conformers of AMA–w, a molecular dynamics approach was used at the GFN2-xTB[18] level of theory using the Conformer-Rotamer Ensemble Sampling Tool (CREST) available in the extended tight binding (xTB) program package.[19,20] This initial search led to 56 possible geometries for AMA–w. All 56 structures were optimized using the dispersion-corrected density functional theory (DFT) B3LYP[21]-D3(BJ)[22,23] functional with Dunning's aug-cc-pVTZ[24] basis set. The B3LYP-D3(BJ)/aug-cc-pVTZ calculations led to 25 unique minima as some of the initial structures converged to the same energy minimum. The relative energies and Cartesian coordinates for these 25 conformers are given in Appendix 5 of the electronic supplementary information (ESI) file. Next, the optimized geometries from B3LYP-D3(BJ) whose relative energies were within 10 kJ mol^{-1} were re-optimized at higher levels of theory including the double hybrid B2PLYP[25] method with D3(BJ)[22,23] dispersion corrections (referred to as B2PLYP-D3 hereafter) and the *ab initio* MP2[26] methods both combined with the aug-cc-pVTZ basis set. It is worth noting that conformers with relative energies larger than 10 kJ mol^{-1} are not expected to be sufficiently populated for observation using our spectroscopic methods. Vibrational frequency calculations within the harmonic approximation were performed for all optimized geometries at the same levels of theory to validate the nature of the stationary points, to compute energies with zero-point corrections (ZPE) and to estimate quartic centrifugal distortion constants. The Boys and Bernardi's counterpoise method[27] was

included in all optimization and frequency calculations to account for basis set superposition (BSSE) error. The optimization and frequency calculations were performed using the Gaussian 16 program.[28]

Non-covalent interaction (NCI),[13] quantum theory of atoms in molecules (QTAIM)[12] and natural bond orbital (NBO, B3LYP-D3(BJ)/aug-cc-pVTZ)[14] analyses were performed to identify and quantify the intra- and intermolecular interactions responsible for the conformers of AMA–w using the NCIPLOT,[29] AIMALL[30] and NBO 7 programs,[31] respectively. The interaction energy between the water and AMA monomers for each observed conformer was further decomposed into physically meaningful terms (electrostatic, exchange or Pauli repulsion, induction and dispersion) using the symmetry-adapted perturbation theory (SAPT)[15] energy decomposition analysis (EDA). For comparison, we also performed EDA for related amine–w complexes and compare the results with with those of the water dimer and ammonia–w. The SAPT calculations were done at the SAPT2+(3)δMP2[32]/aug-cc-pVTZ level using the Psi4 code.[33] Atomic charges were also computed using the Voronoi deformation density (VDD)[34] method as implemented in the Multiwfn software.[35]

Results

Potential Energy Surface

For the AMA monomer itself, a total of nine energy minima were reported[10] on the potential energy surface and were labeled using a Roman numeral from I–IX which describes their decreasing order of stability with I being the most stable geometry. Experimentally, rotational transitions for the four low energy conformers (ΔE_{ZPE} < 2.1 kJ mol^{-1}) I, II, III and V were observed in a supersonic jet expansion and their populations were estimated to be 40%, 36%, 22% and 2%, respectively. Since the interaction with a water molecule may induce changes in the relative energy ordering of the monomer geometries upon complexation, all conformers of AMA must be considered when searching for the energy minima of the AMA–w complex. This is done automatically during the initial steps of the conformational searches in the CREST procedure through the iMTD-GC algorithm which considers all possible orientations of the monomer geometries and binding sites for the water molecule. After the conformational searches, optimizations at higher levels of theory led to nine conformers for AMA–w, depicted in Figure 1, whose relative energies are within 10 kJ mol^{-1}. Although higher energy conformers exist, only those below 10 kJ mol^{-1} are expected to be sufficiently populated for detection by FTMW spectroscopy in a supersonic jet. The atomic coordinates for each of the nine conformers are provided in Tables S1–S9 of the ESI file. Their calculated energetic and spectroscopic parameters from both the B2PLYP-D3 and MP2 methods are given in Table 1. The geometries of the monohydrated complexes were named using the acronym AMA followed by a first Roman numeral which represents the monomer geometry, the letter “w” for water and a second Roman numeral to denote the order of

stability of the complex with AMA-I-w-I being the most stable conformer. Overall, the calculated relative energy orderings, rotational constants (*A*, *B* and *C*), quadrupole coupling constants [$1.5\chi_{aa}$ and $0.25\ (\chi_{bb}- \chi_{cc})$] and electric dipole moment components (μ_a, μ_b, μ_c) for the conformers of AMA–w from the B2PLYP-D3 and MP2 methods are consistent with each other.

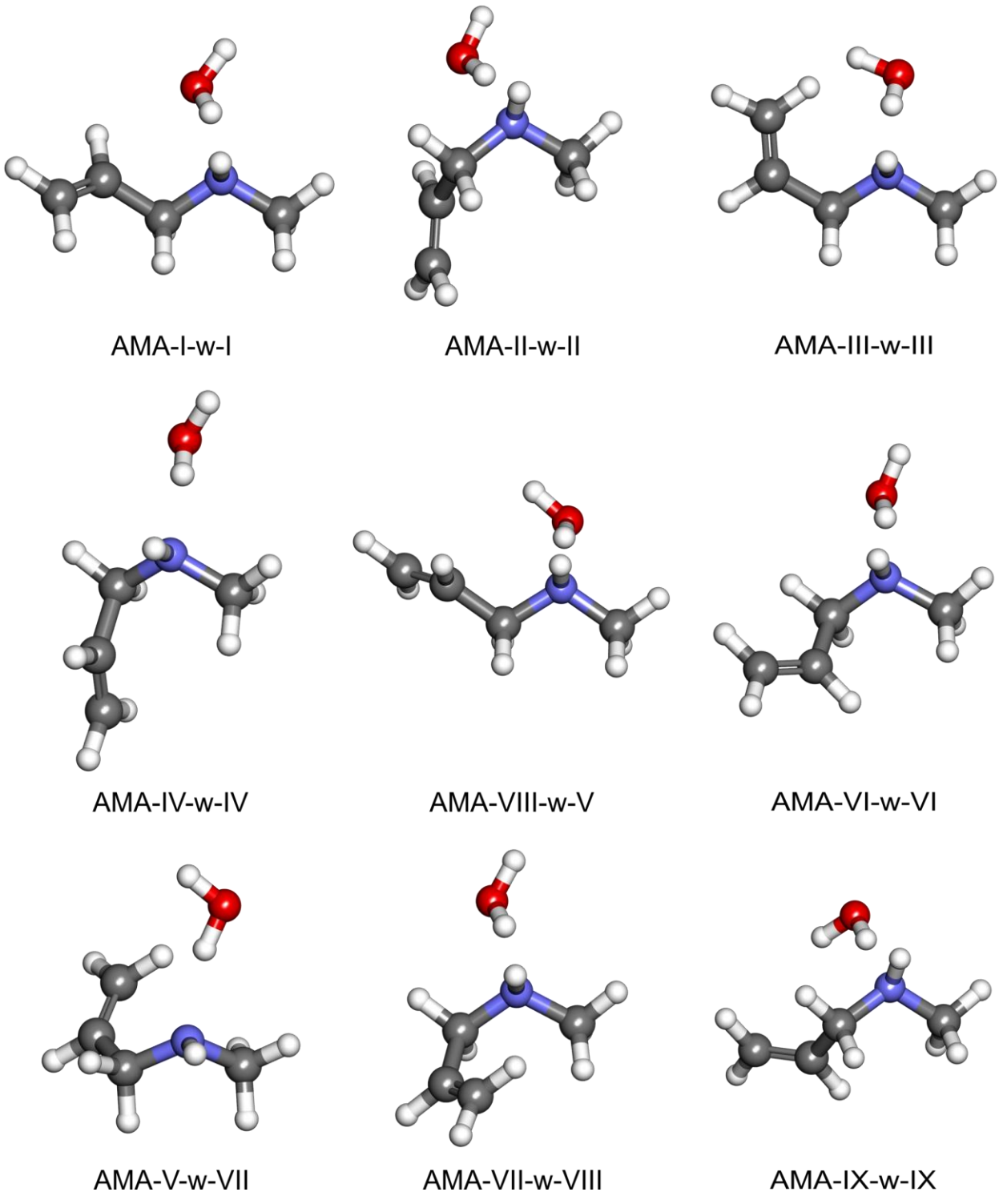

Figure 1. Nine conformers of the AMA–w complex identified within an energy window of 10 kJ mol^{-1} using quantum chemical calculations (B2PLYP-D3/aug-cc-pVTZ).

Table 1. Calculated relative energies with zero-point corrections (ZPE) ΔE_0 in kJ mol^{-1}, population P at 298K in %, rotational (A, B and C) and ^{14}N quadrupole coupling [1.5 (χ_{aa}) and 0.25 (χ_{bb}- χ_{cc})] constants in MHz, and electric dipole moment components (μ_a, μ_b and μ_c) in Debye for the nine most stable conformers of the AMA–w complex obtained at the B2PLYP-D3 and MP2 levels with the aug-cc-pVTZ basis set.

Conformer	B2PLYP-D3					MP2				
	ΔE_0	P_{298K}	$A/B/C$	1.5 (χ_{aa})/0.25 (χ_{bb}- χ_{cc})	$\mu_a/\mu_b/\mu_c$	ΔE_0	P_{298K}	$A/B/C$	1.5 (χ_{aa})/0.25 (χ_{bb}- χ_{cc})	$\mu_a/\mu_b/\mu_c$
AMA-I-w-I	0.0	41.3	3441/1984/1345	1.84/-1.40	0.1/2.5/1.3	0.0	39.4	3504/1998/1365	1.70/-1.26	0.0/2.4/1.3
AMA-II-w-II	1.7	20.9	3255/2134/1568	-0.80/-0.83	0.2/2.9/0.7	1.2	23.8	3260/2167/1594	-1.16/-0.73	0.3/2.9/0.8
AMA-III-w-III	2.5	14.9	3197/2290/1511	3.71/-1.70	2.0/2.6/0.2	2.5	14.2	3298/2277/1559	3.60/-1.64	1.9/2.4/0.3
AMA-IV-w-IV	4.1	8.0	5336/1474/1292	-6.11/0.03	1.7/2.0/1.5	3.7	8.7	5223/1519/1347	-5.87/0.00	1.6/1.9/1.5
AMA-VIII-w-V	5.0	5.4	3361/2105/1400	4.21/-1.79	1.4/2.7/1.0	5.0	5.2	3458/2128/1427	3.99/-1.60	1.1/2.4/1.1
AMA-VI-w-VI	6.1	3.6	4979/1484/1213	-5.18/-0.22	1.8/1.9/1.5	6.5	2.8	5226/1488/1237	-4.80/-0.19	1.8/1.6/1.6
AMA-V-w-VII	6.9	2.5	3288/2232/1656	0.56/-1.30	2.5/1.3/1.3	6.7	2.7	3433/2196/1655	0.83/-1.26	2.2/1.3/1.3
AMA-VII-w-VIII	7.0	2.4	5643/1543/1308	-7.12/0.10	2.0/1.5/1.0	6.9	2.4	5806/1569/1330	-6.60/0.14	1.9/1.4/1.1
AMA-IX-w-IX	9.3	1.0	2919/2375/1528	4.11/-1.70	1.3/3.2/0.2	9.6	0.8	2937/2416/1554	3.88/-1.67	1.4/3.3/0.2

Spectral analysis

The broadband cp-FTMW spectrum of the AMA and water mixture is very dense including lines from the four conformers (I, II, III and V) of the monomer reported previously.[10] Once these known transitions were excluded, two sets of *R*-branch *b*-type transitions were rapidly identified. This suggested the formation of two new species in the supersonic jet with sizeable μ_b dipole components. By comparing the experimental rotational constants with the predicted values for each individual conformer (Table 1), the patterns were assigned to the parent species of the two most stable conformers predicted for the complex, AMA-I-w-I and AMA-II-w-II. The initial assignments were confirmed using the BF-FTMW instrument which allowed the ^{14}N hyperfine structure to be better resolved. No extra tunneling splittings due to methyl internal rotation or N–H inversion within AMA (as seen for the monomer)[10] or to the movement of the water subunit were observed. A portion of the cp-FTMW spectrum of AMA–w is given in Figure 2 while the BF-FTMW spectrum for the 6_{16}-5_{05} transition of AMA-I-w-I highlighting ^{14}N hyperfine components is provided in Figure 3.

The final fitting of all measured transitions was carried out with Pickett's SPFIT program[36] using Watson's S-reduced Hamiltonian[37] (I^r representation) to obtain accurate rotational, quartic centrifugal distortion and quadrupole coupling constants. A summary of the resulting values is given in Table 2. The consistency with the theoretical predictions in Table 1 confirms the assignment of conformers AMA-I-w-I and AMA-II-w-II. The complete line lists of measured transitions and residuals are provided in Tables S10-S11. No transitions belonging to other AMA–w species were detected which may be a consequence of insufficient population or relaxation to lower energy forms.

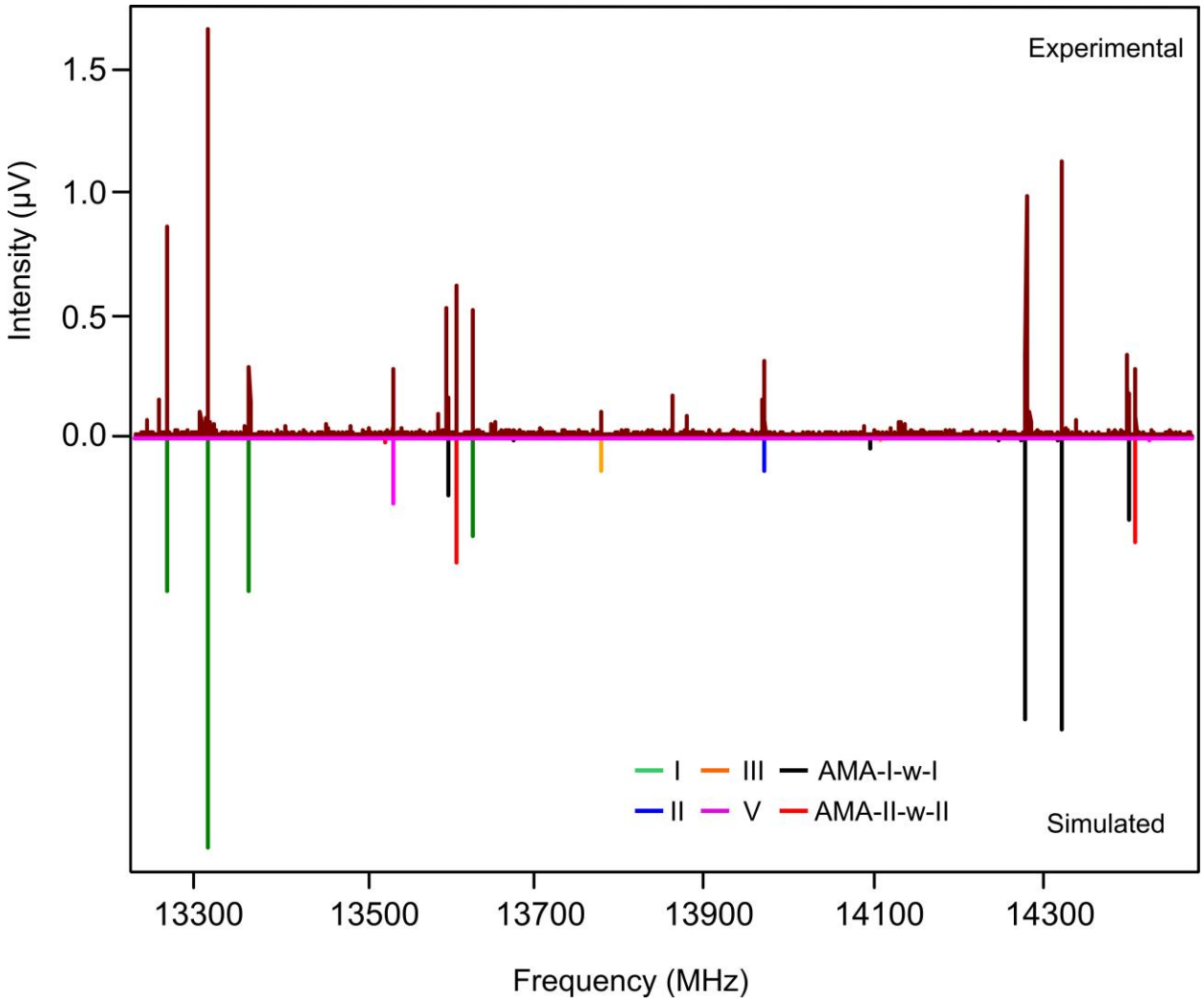

Figure 2. Section of the cp-FTMW spectrum (1.5 million FIDs). The upper trace (maroon) represents the experimental spectrum while the lower traces (in colour) show simulations of the spectra of the known conformers of AMA and AMA–w. The intensity of the simulated transitions is based on calculated electric dipole moment components and populations.

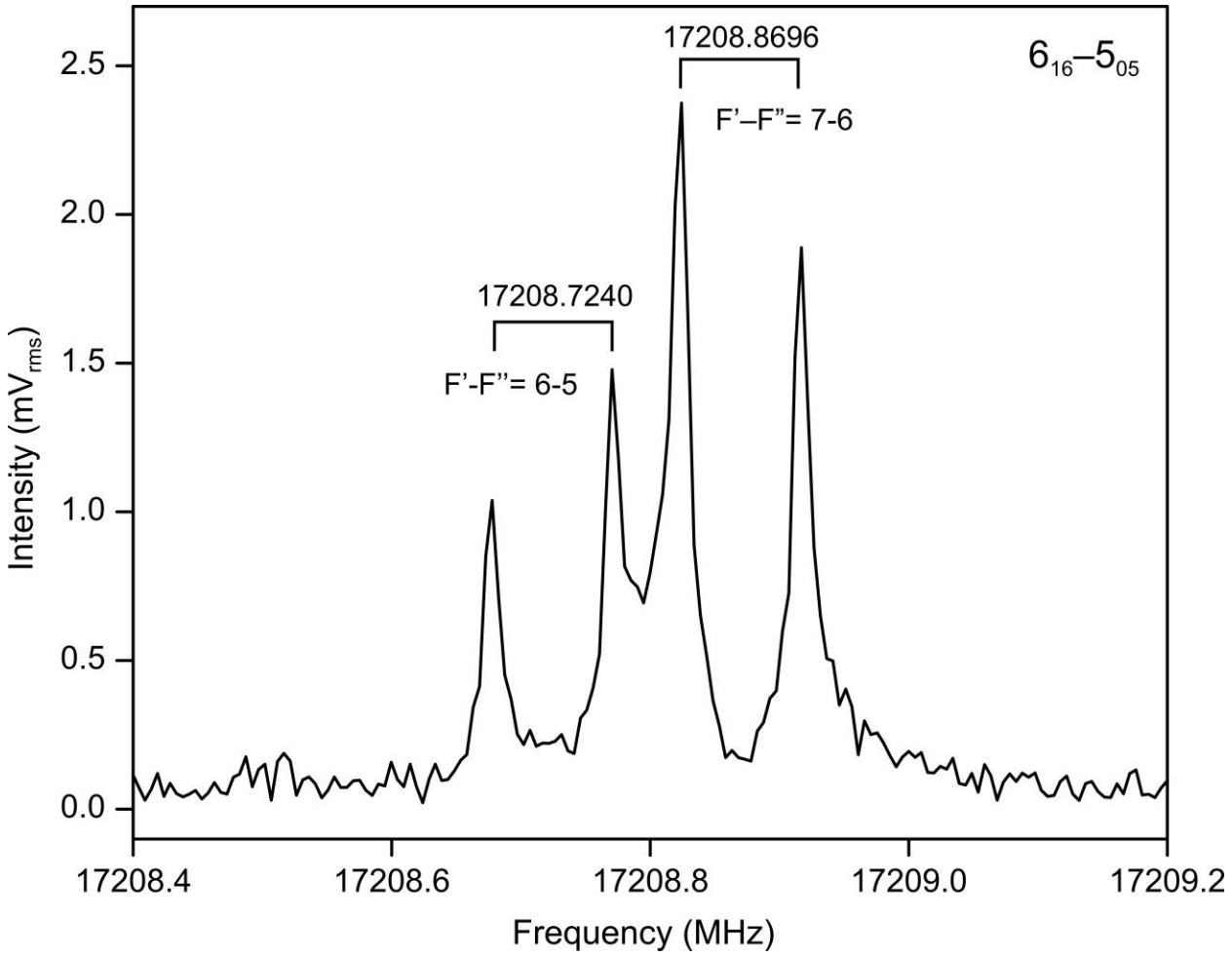

Figure 3. BF-FTMW spectrum for the 6_{16}–5_{05} rotational transition of conformer AMA-I-w-I highlighting two ^{14}N hyperfine components.

Table 2. Experimentally derived spectroscopic parameters for the two observed conformers of the AMA–w complex.

Parameter	AMA-I-w-I	AMA-II-w-II
A/MHz[a]	3442.84817(33)	3260.33627(73)
B/MHz	1959.50815(24)	2082.50939(77)
C/MHz	1330.95365(11)	1542.36365(25)
D_J/kHz[b]	2.6641(44)	3.423(12)
D_{JK}/kHz	-3.171(20)	-4.470(65)
D_K/kHz	29.706(35)	12.879(78)
d_1/kHz	-1.3021(31)	-1.059(12)
d_2/kHz	-0.2410(21)	-0.041(11)
1.5 (χ_{aa})/MHz[c]	1.6642(37)	-0.9239(67)
0.25 (χ_{bb}- χ_{cc})/MHz	-1.31271(70)	-0.7976(11)
$\mu_a/\mu_b/\mu_c$[d]	n/y/y	n/y/n
N[e]	82	36
σ/kHz[f]	2.1	2.1

[a]Rotational constants; [b]quartic centrifugal distortion constants; [c]^{14}N nuclear quadrupole coupling constants; [d]electric dipole moment components (“y” if observed and “n” if not observed); [e]total number of lines (N) in the fit; [f]root-mean-square deviation of the fit (σ). The full set of calculated constants at both B2PLYP-D3 and MP2 methods are provided in Table S12.

Discussion

All nine AMA–w conformers, identified by the B2PLYP-D3 and MP2 calculations, are stabilized by a primary N···H–O intermolecular HB in which the nitrogen atom serves as a HB acceptor while the water molecule acts as a HB donor (Figure 1). This is consistent with the greater nucleophilic character of nitrogen compared to that of oxygen. The favoured HB acceptor role of nitrogen has also been highlighted in previous studies

dealing with the monohydrated complexes of primary, secondary and tertiary amines such as MA–w,[5] DMA–w,[4–6] TMA–w,[4,5,7] PA–w and IPA–w.[9] Depending on the geometry adopted by the AMA monomer, the water molecule can simultaneously act as a HB acceptor as in conformers AMA-I-w-I and AMA-II-w-II where a secondary C–H···O HB is established between the vinylic hydrogen and the oxygen atom of water. The nature and strength of the intermolecular interactions occurring in the conformers of AMA–w will be discussed in detail below.

The relative energy ordering for the four most stable geometries of AMA–w follows the same trend observed in the isolated amine.[10] Significant changes are observed, however, in the stability ordering of higher energy conformers following complexation. This is exemplified, for example, by the stabilization of the eighth most stable conformer of the AMA monomer to form the fifth most stable hydrate (AMA-VIII-w-V) and by the destabilization of the AMA monomer V to form AMA-V-w-VII. In this sense, interactions with water disrupt the conformational equilibrium of AMA to some extent with the effects being most pronounced for AMA species lying ~5 kJ mol^{-1} or more above the global minimum. The detection of AMA-I-w-I and AMA-II-w-II confirms that the intramolecular interactions responsible for the low energy conformers I (40%) and II (36%) of AMA remain important in the presence of water while higher energy dimers were not produced in sufficient quantities to be detected despite their sizeable dipole moments (Table 1).

To understand why conformers AMA-I-w-I and AMA-II-w-II are the two most stable complexes, one must explore the intrinsic nature of the interactions responsible for these geometries. As the calculated rotational constants from B2PLYP-D3/aug-cc-pVTZ for AMA-I-w-I and AMA-II-w-II matched the experimental ground state values, it is reasonable

to assume that the equilibrium structures at this level of theory provide a good description of these conformers. The HB parameters extracted from the equilibrium structures, namely the N···H–O and C–H···O distances, are 1.89Å and 2.76Å, and 1.91Å and 2.57Å in conformers AMA-I-w-I and AMA-II-w-II, respectively. This suggests that the strength of the N···H–O interaction is similar in AMA-I-w-I and AMA-II-w-II (slightly shorter N···H–O distance in AMA-I-w-I) while the secondary C–H···O interaction is more favoured in AMA-II-w-II based on the shorter HB. To further characterize the underlying effects leading to such subtle differences, we used the three well-known QTAIM, NCI and NBO approaches.

The QTAIM molecular plots and associated parameters for the nine conformers of AMA–w are given in Figure S1 and Table S13, respectively. These show that all conformers exhibit a primary N···H–O HB as evidenced by the presence of a bond critical point (BCP, green dot) along the interaction path between the nitrogen and hydrogen atoms. In addition, AMA-I-w-I, AMA-II-w-II and AMA-V-w-VII display a secondary C–H···O HB. Using the electronic potential energy at the BCP, V_{BCP}, the strength of each HB can be obtained by $E_{HB} = 0.5V_{BCP}$.[38] The energies of the primary N···H–O and secondary C–H···O HBs in the different conformers vary from -37 to -39 kJ mol^{-1} and from -4 to -6 kJ mol^{-1}, respectively. When focusing on the QTAIM graphs of the two observed conformers (Figure 4A), the primary contact is indeed stronger in AMA-I-w-I than in AMA-II-w-II (by ~1.2 kJ mol^{-1}) while the reverse is true for the secondary interaction (~1.1 kJ mol^{-1} stronger in AMA-II-w-II) in agreement with the aforementioned HB distances. Nevertheless, the overall contribution from these intermolecular HBs to the stabilization of the two lowest energy conformers seem to cancel each other implying that their relative energy

difference is not solely dependent on the strength of the intermolecular contacts but also on stabilizing and destabilizing intramolecular effects within the monomers themselves.

While the QTAIM approach is useful to characterize short to medium range HBs, NCI calculations can identify weaker interactions.[39] The NCI results, shown in Figure S2 for all conformers and in Figure 4B for AMA-I-w-I and AMA-II-w-II, confirm the strong N···H–O HB (blue coloured surfaces in the interacting regions) in all conformers and a weaker C–H···O HB (green coloured isosurfaces) in AMA-I-w-I, AMA-II-w-II and AMA-V-w-VII. The NCI outcomes also identify weaker secondary C–H···O contacts in AMA-III-w-III and AMA-VIII-w-V which were not captured by the QTAIM method. The intramolecular forces are similar to those first identified in the isolated molecule[10] in most of the conformers of AMA–w (specifically in the four lowest energy ones), lending support to the notion that these internal interactions are the primary influencers of the relative energy ordering of the most stable hydrates. Interestingly, complexation with water alters the nature of the intramolecular contacts in the higher energy forms of AMA and disrupts their stability ordering in agreement with the DFT and MP2 calculations. A noteworthy example arises from the comparison of the previously reported NCI plot of AMA conformer V (ref [10]) with the one of its monohydrate AMA-V-w-VII (Figure S2, this work). Although the monomer geometry within the complex is largely maintained, the HBs established with water in AMA-V-w-VII leads to the formation of a 7-membered ring (involving atoms from the amino and allyl groups) resulting in the appearance of attractive and repulsive isosurfaces (absent in the isolated AMA conformer V). It is evident from the relative energy of the complex, that the combination of these effects leads to overall destabilization within the AMA V partner itself as the strength of the intermolecular

contacts (Table S13, QTAIM) with water are actually greater than in some of the other hydrates. In contrast, the formation of a longer-range C–H···O HB in AMA-VIII-w-V does not lead to new destabilizing intramolecular interactions within conformer VIII (Figure S2) but suggests that this weak secondary contact (not captured by QTAIM) is sufficient to bind the water molecule preferentially to monomer geometry VIII over others (namely V, VI, VII) based on the relative energies in Table 1. These two examples highlight the disruptive role that water can play through complex subtle effects that ultimately rule the conformational landscape of the AMA–w.

The results from the topological QTAIM and NCI analyses for the observed conformers are inline with NBO calculations in which charge transfer between electron donor (lone-pair) and acceptor (σ*) orbitals corresponding to these interactions is found to contribute to their second-order perturbation energies $E^{(2)}$. A summary of the NBO results for conformers AMA-I-w-I and AMA-II-w-II is given in Table S14.

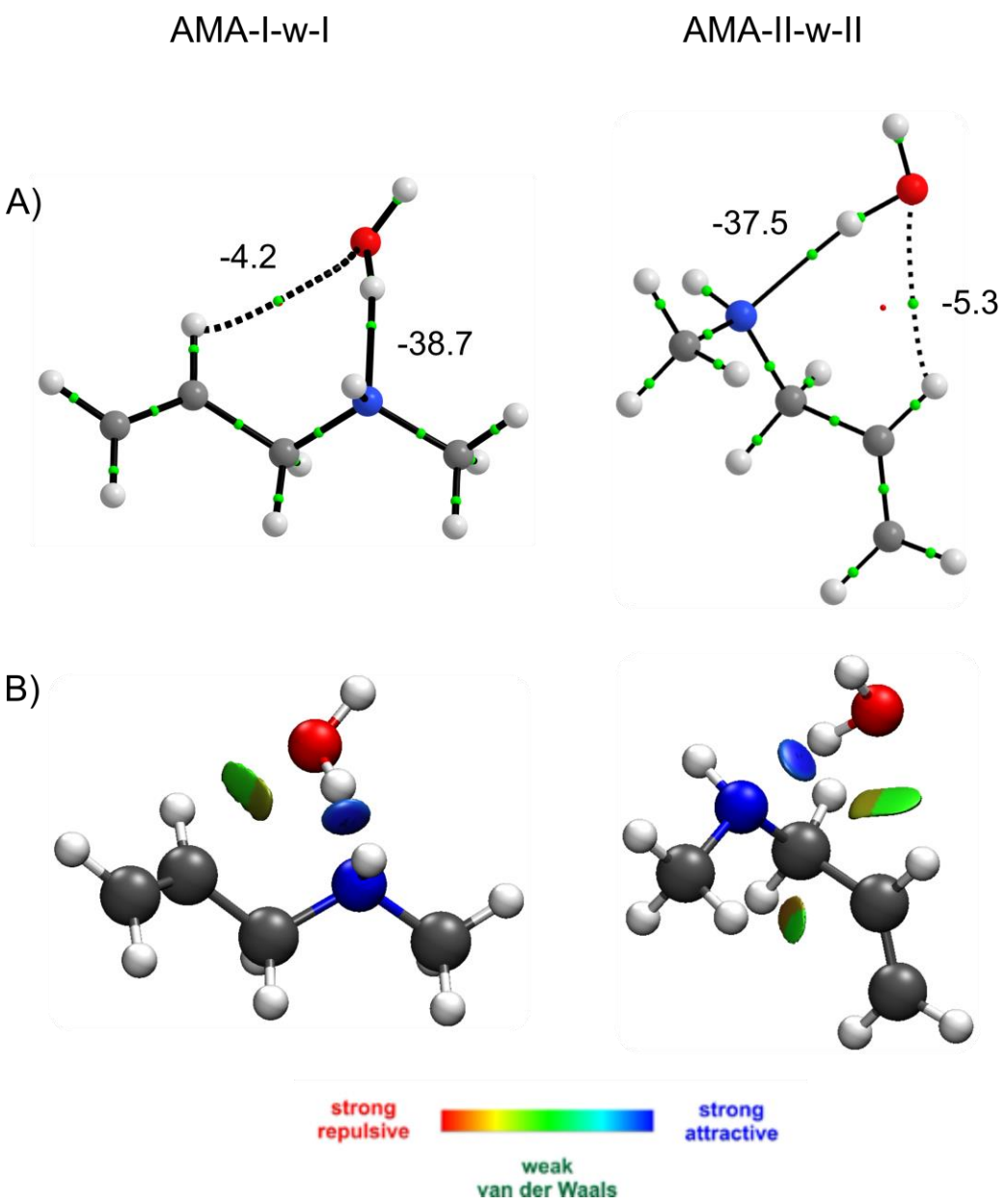

Figure 4. A) QTAIM molecular graphs containing the energies (in kJ mol^{-1}) for the N···H–O and C–H···O HB and B) NCI isosurfaces (s=0.5 and colour scale BGR: 0.02 < ρ < +0.02) for the two observed conformers of the AMA–w complex.

Once the individual intra- and intermolecular interactions were identified, to understand the physical origins behind the formation of the AMA–w complex, the interaction energies (E_{total}) were decomposed using the SAPT analysis at the SAPT2+(3)δMP2/aug-cc-pVTZ level of theory as summarized in Table 3. The SAPT results confirm the slightly greater stability of AMA-I-w-I (larger negative E_{total} value) over AMA-II-w-II. For both, the largest stabilizing contribution is the electrostatic term which is related to favourable Coulombic interactions occurring between the negative charges around the nitrogen (-0.137 in AMA-I-w-I and -0.134 in AMA-II-w-II) and oxygen atoms (-0.307 in AMA-I-w-I and -0.306 in AMA-II-w-II) with the positive atomic charges surrounding the hydrogens (+0.096 and +0.047 in AMA-I-w-I and +0.092 and +0.051 in AMA-II-w-II) involved in the N···H–O and C–H···O HB, respectively. The induction and dispersion terms further stabilize the AMA–w complex but their contributions are approximately three times smaller than the electrostatic one. The difference in the E_{total} between AMA-I-w-I and AMA-II-w-II arises from the destabilizing Pauli repulsion term (exchange) which is smaller in AMA-I-w-I.

Finally, to evaluate the impact of different substituents on the interaction energies of amine–w complexes, we compared the SAPT results from AMA–w with those of other amine monohydrates and with the ammonia–w adduct and the water dimer (Table 3). It is apparent that even the simplest ammonia–w complex has an interaction energy E_{total} that is ~1.3 times stronger than the water dimer suggesting that in water rich environments, such as the Earth's atmosphere, a water molecule binds preferentially to ammonia over self-aggregation. When the hydrogen atoms of ammonia are substituted by methyl groups in a stepwise fashion from MA to TMA, a gradual increase in the stability

(smaller E_{total}) of the complexes is observed with TMA–w being the most stable of this family. It is interesting to note that while AMA is a secondary amine like DMA, the E_{total} for conformer AMA-I-w-I is 1.6 kJ mol^{-1} stronger than in DMA–w and also more stable by 1.4 kJ mol^{-1} than the tertiary amine complex TMA–w. The greater stability of AMA–w in comparison with DMA-w is mainly caused by a slight increase in the contributions from dispersion (Table 3) which is likely from the secondary long-range C–H···O HB established with the vinyl group in AMA–w. On the other hand, the surprisingly larger stability of AMA–w compared to TMA–w is not governed by the stabilizing contributors but rather by the Pauli repulsion term. While the sum of the three stabilizing terms is -107.4 kJ mol^{-1} in TMA–w and -105.8 kJ mol^{-1} in AMA–w, TMA–w is 3.0 kJ mol^{-1} more destabilized by Pauli repulsion (Table 3) by comparison. These subtle differences observed in the stabilizing and destabilizing effects within the clusters in Table 3 reinforce the importance of evaluating the impact of different side chains on the formation of amine–w complexes. A comprehensive conformational study of the homologous series of complexes including, for example, allyamine-water and dimethyallylamine-water would provide interesting insights in this regard.

Table 3. Symmetry-adapted perturbation theory (SAPT) results, in kJ mol^{-1}, (SAPT2+(3)δMP2/aug-cc-pVTZ) for the two observed conformers of AMA–w and related complexes.

Complex	E_{total}	$E_{electrostatic}$	$E_{exchange}$	$E_{induction}$	$E_{dispersion}$
AMA-I-w-I	-34.3	-60.5	71.5	-23.0	-22.3
AMA-II-w-II	-33.6	-60.6	72.3	-22.9	-22.4
TMA-w	-32.9	-61.0	74.5	-24.9	-21.5
DMA-w	-32.7	-59.6	70.2	-23.5	-19.7
MA-w	-31.0	-56.3	64.0	-21.5	-17.2
ammonia-w[a]	-27.2	-49.1	53.0	-17.5	-13.6
water dimer[a]	-20.8	-34.7	35.2	-11.0	-10.3

[a]From reference [40].

Conclusions

The conformational landscape and the intermolecular interactions stabilizing the monohydrated complexes of AMA were revealed in this work for the first time using rotational spectroscopy. Aided by DFT and *ab initio* MP2 predictions, transitions for the two most stable conformers (AMA-I-w-I and AMA-II-w-II) were unequivocally assigned and their hyperfine splittings owing to the ^{14}N quadrupolar nucleus were resolved. In the observed complexes, the water molecule interacts with AMA as both a HB donor and acceptor forming primary N···H–O and a secondary C–H···O HBs on the order of -37 to -39 kJ mol^{-1} and -4 to -6 kJ mol^{-1}, respectively. While the formation of HBs with water are not sufficient to overcome the internal forces governing the conformational landscape of the most stable monomers, they certainly affect the intramolecular interactions responsible for the energy ordering of higher energy conformations. Based on the energy components identified via SAPT analysis, the nature of the complex formation is mainly electrostatic with smaller contributions from induction and dispersion. By comparing the results for AMA–w with those from the water dimer, ammonia–w, MA–w, DMA–w and TMA–w clusters, we show that AMA is more readily hydrated. Relative to other primary and secondary amines, the presence of the vinyl group in AMA favours the formation of secondary contacts such as the C–H···O HB and thus tunes the overall interaction energy. For the tertiary case of TMA–w, the fewer substituents at N in AMA offer less stabilizing effects in comparison but the reduced exchange term in AMA–w yields greater stability overall. In closing, this study highlights the need for enhanced understanding of the unique influences that govern the interactions between amines and water on a microscopic scale including the number and identity of the organic sidechains and lays groundwork for modelling their chemistry in atmospheric and biological processes.

Electronic Supplementary Information (ESI)

Appendix 1: Cartesian coordinates for the nine conformers of the AMA–w complex

Appendix 2: Assigned transitions and residuals for the observed conformers of AMA–w

Appendix 3: Full set of calculated spectroscopic parameters for conformers AMA-I-w-I and AMA-II-w-II

Appendix 4: QTAIM, NCI and NBO analyses for the conformers of AMA–w

Appendix 5: Relative energies and Cartesian coordinates for the 25 energy minima at B3LYP-D3(BJ)/aug-cc-pVTZ

Conflicts of interest

There are no conflicts to declare.

Acknowledgements

The authors thank the Natural Sciences and Engineering Research Council of Canada (NSERC) for funding this research through the Discovery Grants program and the University of Manitoba for its computing facility (GREX). W.G.D.P.S and T.P. are grateful for financial support provided through a University of Manitoba Graduate Fellowship and the GETS program, respectively, subsidized both by the Faculty of Graduate Studies.

References

1 X. Ge, A. S. Wexler and S. L. Clegg, *Atmos. Environ.*, 2011, **45**, 524–546.

2 P. Herbine and T. R. Dyke, *J. Chem. Phys.*, 1985, **83**, 3768–3774.

3 A. Engdahl and B. Nelander, *J. Chem. Phys.*, 1989, **91**, 6604–6612.

4 A. Kjaersgaard, E. Vogt, A. S. Hansen and H. G. Kjaergaard, *J. Phys. Chem. A*, 2020, **124**, 7113–7122.

5 B. T. Mmereki and D. J. Donaldson, *J. Phys. Chem. A*, 2002, **106**, 3185–3190.

6 M. J. Tubergen and R. L. Kuczkowski, *J. Mol. Struct.*, 1995, **352**, 335–344.

7 M. J. Tubergen and R. L. Kuczkowski, *J. Am. Chem. Soc.*, 1993, **115**, 9263–9266.

8 M. Rozenberg, A. Loewenschuss and C. J. Nielsen, *J. Phys. Chem. A*, 2012, **116**, 4089–4096.

9 J. Chen, Y. Zheng, A. Melli, L. Spada, T. Lu, G. Feng, Q. Gou, V. Barone and C. Puzzarini, *Phys. Chem. Chem. Phys.*, 2020, **22**, 5024–5032.

10 W. G. D. P. Silva, T. Poonia and J. Wijngaarden, *ChemPhysChem*, 2020, **21**, 2515–2522.

11 P. Vitins and K. W. Egger, *J. Chem. Soc., Perkin Trans. 2*, 1974, 1289–1291.

12 R. F. W. Bader, *Acc. Chem. Res.*, 1985, **18**, 9–15.

13 E. R. Johnson, S. Keinan, P. Mori-Sánchez, J. Contreras-García, A. J. Cohen and W. Yang, *J. Am. Chem. Soc.*, 2010, **132**, 6498–6506.

14 F. Weinhold, C. R. Landis and E. D. Glendening, *Int. Rev. Phys. Chem.*, 2016, **35**, 399–440.

15 B. Jeziorski, R. Moszynski and K. Szalewicz, *Chem. Rev.*, 1994, **94**, 1887–1930.

16 L. Evangelisti, G. Sedo and J. van Wijngaarden, *J. Phys. Chem. A*, 2011, **115**, 685–690.

17 G. Sedo and J. van Wijngaarden, *J. Chem. Phys.*, 2009, **131**, 044303.

18 C. Bannwarth, S. Ehlert and S. Grimme, *J. Chem. Theory Comput.*, 2019, **15**, 1652–1671.

19 S. Grimme, *J. Chem. Theory Comput.*, 2019, **15**, 2847–2862.

20 P. Pracht, F. Bohle and S. Grimme, *Phys. Chem. Chem. Phys.*, 2020, **22**, 7169–7192.

21 A. D. Becke, *J. Chem. Phys.*, 1993, **98**, 5648–5652.

22 S. Grimme, S. Ehrlich and L. Goerigk, *J. Comput. Chem.*, 2011, **32**, 1456–1465.

23 S. Grimme, J. Antony, S. Ehrlich and H. Krieg, *J. Chem. Phys.*, 2010, **132**, 154104.

24 T. H. Dunning, *J. Chem. Phys.*, 1989, **90**, 1007–1023.

25 S. Grimme, *J. Chem. Phys.*, 2006, **124**, 034108.

26 C. Møller and M. S. Plesset, *Phys. Rev.*, 1934, **46**, 618–622.

27 S. F. Boys and F. Bernardi, *Mol. Phys.*, 1970, **19**, 553–566.

28 M. J. Frisch, G. W. Trucks, H. B. Schlegel, G. E. Scuseria, M. A. Robb, J. R.

Cheeseman, G. Scalmani, V. Barone, G. A. Petersson, H. Nakatsuji, X. Li, M. Caricato, A. V. Marenich, J. Bloino, B. G. Janesko, R. Gomperts, B. Mennucci, H. P. Hratchian, J. V. Ortiz, A. F. Izmaylov, J. L. Sonnenberg, D. Williams-Young, F. Ding, F. Lipparini, F. Egidi, J. Goings, B. Peng, A. Petrone, T. Henderson, D. Ranasinghe, V. G. Zakrzewski, J. Gao, N. Rega, G. Zheng, W. Liang, M. Hada, M. Ehara, K. Toyota, R. Fukuda, J. Hasegawa, M. Ishida, T. Nakajima, Y. Honda, O. Kitao, H. Nakai, T. Vreven, K. Throssell, J. A. Montgomery, Jr., J. E. Peralta, F. Ogliaro, M. J. Bearpark, J. J. Heyd, E. N. Brothers, K. N. Kudin, V. N. Staroverov, T. A. Keith, R. Kobayashi, J. Normand, K. Raghavachari, A. P. Rendell, J. C. Burant, S. S. Iyengar, J. Tomasi, M. Cossi, J. M. Millam, M. Klene, C. Adamo, R. Cammi, J. W. Ochterski, R. L. Martin, K. Morokuma, O. Farkas, J. B. Foresman, and D. J. Fox, Gaussian 16 (Revision C.01), Gaussian, Inc., Wallingford, CT, 2016.

29 J. Contreras-García, E. R. Johnson, S. Keinan, R. Chaudret, J.-P. Piquemal, D. N. Beratan and W. Yang, *J. Chem. Theory Comput.*, 2011, **7**, 625–632.

30 T. A. Keith, AIMAll (Version 17.11.14), TK Gristmill Software, Overland Park, KS, 2016.

31 E. D. Glendening, J. K. Badenhoop, A. E. Reed, J. E. Carpenter, J. A. Bohmann, C. M. Morales, P. Karafiloglou, C. R. Landis, and F. Weinhold, NBO 7.0, Theoretical Chemistry Institute, University of Wisconsin, Madison, WI, 2018.

32 E. G. Hohenstein and C. D. Sherrill, *J. Chem. Phys.*, 2010, **133**, 014101.

33 R. M. Parrish, L. A. Burns, D. G. A. Smith, A. C. Simmonett, A. E. DePrince, E. G. Hohenstein, U. Bozkaya, A. Y. Sokolov, R. Di Remigio, R. M. Richard, J. F.

Gonthier, A. M. James, H. R. McAlexander, A. Kumar, M. Saitow, X. Wang, B. P. Pritchard, P. Verma, H. F. Schaefer, K. Patkowski, R. A. King, E. F. Valeev, F. A. Evangelista, J. M. Turney, T. D. Crawford and C. D. Sherrill, *J. Chem. Theory Comput.*, 2017, **13**, 3185–3197.

34 C. Fonseca Guerra, J. W. Handgraaf, E. J. Baerends and F. M. Bickelhaupt, *J. Comput. Chem.*, 2004, **25**, 189–210.

35 T. Lu and F. Chen, *J. Comput. Chem.*, 2012, **33**, 580–592.

36 H. M. Pickett, *J. Mol. Spectrosc.*, 1991, **148**, 371–377.

37 J. K. G. Watson, *in Vibrational Spectra and Structure*, ed. J. R. Durig, Elsevier, New York, vol. 6, 1977.

38 E. Espinosa, E. Molins and C. Lecomte, *Chem. Phys. Lett.*, 1998, **285**, 170–173.

39 J. R. Lane, J. Contreras-García, J. P. Piquemal, B. J. Miller and H. G. Kjaergaard, *J. Chem. Theory Comput.*, 2013, **9**, 3263–3266.

40 S. Emamian, T. Lu, H. Kruse and H. Emamian, *J. Comput. Chem.*, 2019, **40**, 2868–2881.